Collapse of a bubble injected side-by-side with another bubble into an incipiently fluidized bed: A CFD-DEM study

A. Padash and C. M. Boyce*
Department of Chemical Engineering, Columbia University, New York, New York 10027, USA

(Received 25 October 2019; accepted 11 February 2020; published 16 March 2020)

A recent magnetic resonance imaging study [Boyce *et al.*, Phys. Rev. Fluids **4**, 034303 (2019)] found that when two bubbles were injected side-by-side into an incipiently fluidized bed, below a critical injection volume, one bubble collapsed, while the other bubble survived, reaching the bed surface. Limitations in the experimental measurements left open questions about the apparent collapse: (1) did the bubble actually collapse or rather move out of the imaging plane and (2) if the bubble collapsed, was it due to gas transfer between bubbles or a preference for gas to channel toward the surviving bubble. Here we demonstrate that computational fluid dynamics–discrete element method (CFD-DEM) simulations can recreate this phenomenon. Simulation results reveal that the bubble does in fact collapse and that this collapse occurs because the slight size difference between the two bubbles causes gas flow to channel preferentially to the larger bubble, leaving the smaller bubble without enough gas flow to support its roof.

DOI: 10.1103/PhysRevFluids.5.034304

I. INTRODUCTION

Voids or "bubbles" in fluidized granular beds create fascinating scientific questions due to their similarities in shape and rise behavior to bubbles in conventional fluids, despite the fact that there is no interface or surface tension between the void and particle-laden regions and gas passes freely between both regions [1,2]. Further, bubbles are critical to a variety of industrial processes involving fluidized beds, since bubbles are the main cause of particle mixing and convection, promoting uniform temperature, and bubbles provide a path for gas to largely bypass interaction with particles, limiting gas-particle heat and mass transport [3]. Thus, bubbles in fluidized beds have been the attention of longstanding and focused study in engineering and physics.

Recently Boyce *et al.* [4] published an experimental magnetic resonance imaging (MRI) study, reporting the collapse, or volume abruptly reaching zero, of a bubble injected into an incipiently fluidized bed when a neighboring second bubble was injected simultaneously. Prior studies have shown bubbles collapsing in systems with internal obstacles [5], but the findings of Boyce *et al.* [4] were the first demonstration known to the authors of bubble collapse related to bubble interaction. When two bubbles were injected simultaneously for the same period of time, one bubble always collapsed and it varied randomly which of the two bubbles collapsed, suggesting the manifestation of an instability. Further, when only a single bubble was injected, the bubble did not collapse. As shown in Fig. 1, reproduced from Boyce *et al.* [4], the authors hypothesized that bubble collapse occurred due to one bubble being slightly smaller than the other, and the smaller bubble receiving less flow through it than the larger bubble because the larger bubble provides a higher permeability to gas flow than the smaller one. As known since the landmark theoretical work of Davidson [1],

*Corresponding author: cmb2302@columbia.edu

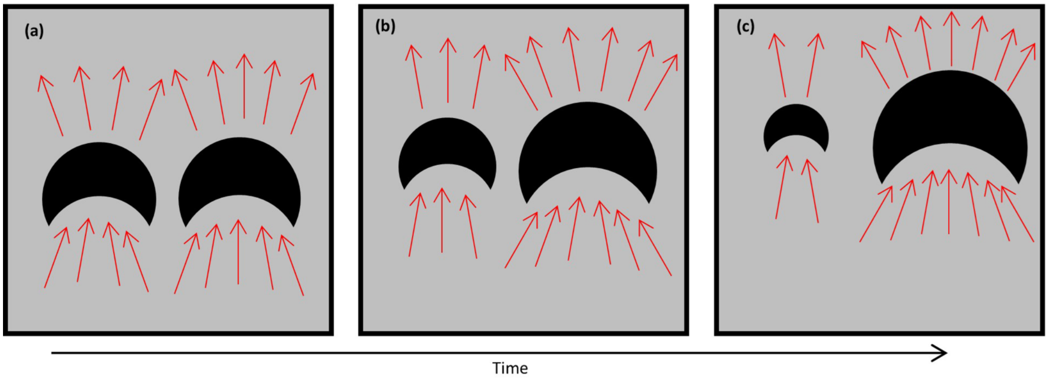

FIG. 1. Schematic copied from the prior experimental study [4], showing the proposed mechanism for bubble collapse, with one bubble starting out slightly smaller than the other and decreasing in size until collapse because a smaller amount of gas flow (shown in red arrows) channels to the smaller bubble, making it unable to maintain the shape of its roof.

gas bubbles require sufficient gas to flow through their roof to maintain their shape. Thus, without sufficient gas flow through its roof, the smaller bubble would decrease in size, and as it decreased in size, less and less gas would channel towards it, causing the decrease in size to continue until its collapse.

This hypothesis for the mechanism underlying the observed collapse is physically sound; however, a number of questions and counterhypotheses surrounded the hypothesis which could not be addressed directly with MRI measurements:

(1) Did the bubble actually collapse, or did it simply move out of the two-dimensional (2D) MRI imaging plane in the three-dimensional (3D) fluidized bed?

(2) Does one bubble actually have to be smaller than the other for collapse to occur, since to the best control of the experiments the bubbles were the same size, and which bubble collapsed varied from experiment to experiment?

(3) Is the mechanism actually related to gas channeling below the two bubbles, or could it be related to gas transfer from the collapsing to the surviving bubble more directly?

These questions largely stem from the fact that the MRI measurements were conducted in a single central plane and did not measure gas velocity. Here we use the Computational Fluid Dynamics–Discrete Element Method (CFD-DEM) [6] simulations, which model the motion of each individual particle using Newtonian and contact mechanics [7] and couple the particle motion to a CFD model of gas flow [8] via a drag law [9], to address these questions and identify the mechanism underlying bubble collapse.

II. METHODS

A. CFD-DEM simulations

CFD-DEM simulations were conducted using the open source platform CFDEMcoupling [10], which models gas flow using the CFD software OpenFOAM [11] and models particle motion using the DEM software LIGGGHTS [12]. A full description of the equations used is described in a previous paper from the corresponding author [13].

The motion of each granular particle was modeled based on contact and Newtonian mechanics using DEM [7]. Table I summarizes the DEM parameters used. A Hertzian spring model was used for normal and tangential contacts with a coefficient of restitution set to 0.69, matching the experimental value. To avoid using excessively small DEM time steps, the particles were simulated as being less stiff than they are in reality, which is used almost universally in CFD-DEM simulations

TABLE I. Discrete element model (DEM) parameters used in CFD-DEM simulations.

Parameter	Value
Tapped bed height, H_0	200 mm
Bed diameter, D_{bed}	190 mm
Particle shape	Spherical
Particle diameter, d_p	2.93 ± 0.04 mm
Particle density	1040 kg/m^3
Coefficient of restitution	0.69
Coefficient of interparticle friction	0.56
Particle-wall friction coefficient	0.56
Poisson's ratio	0.32
Young's modulus	10 MPa
Spring model	Hertzian
DEM time step	0.001 ms

and has been shown to not impact flow significantly [13]. Coulomb's law was used to account for sliding, with a coefficient of friction for particle-particle interactions of 0.56 based on the experimental value.

The gas phase was modeled as a continuum, using CFD with a discretized form of the volume-averaged fluid equations used to solve for gas velocity and pressure on a colocated fluid grid. Table II summarizes the CFD parameters. To allow for longer CFD time steps, an incompressible code with an implicit solver was used. To match the cylindrical experimental geometry, an unstructured grid was used with rectangular cells used in the center of the system and wedge-shaped cells near the walls. Figure 2 shows a horizontal cross section of the mesh used. The vertical-direction grid spacing was $dz = 9.375$ mm and $dx = dy = 9.047$ mm was used for the square grid cells far from the boundaries in the horizontal direction, between three and four particle diameters, matching recommendations for accurate and grid-independent simulation results [14–16].

The two phases were coupled using the drag law of Wen and Yu [9].

B. Fluidized bed

The fluidized bed simulated was identical to that used in the previous MRI experiment [4]: it was 190 mm in diameter and 300 mm in height. The particle diameter was 2.93 ± 0.04 mm, and density was 1040 kg/m^3, to match those measured for the experimental particles. The minimum fluidization velocity used to barely suspend the particles in both the experiments and the simulations was 0.70 m/s.

TABLE II. CFD parameters used in CFD-DEM simulations.

Parameter	Value
Overall height of simulation	300 mm
Bed diameter, D_{bed}	190 mm
Fluid grid spacing	9.375 mm
Superficial velocity, U	0.70 m/s
Distance between injection ports	72.4 mm
Wall boundary condition	No slip
Outlet boundary condition	Constant pressure

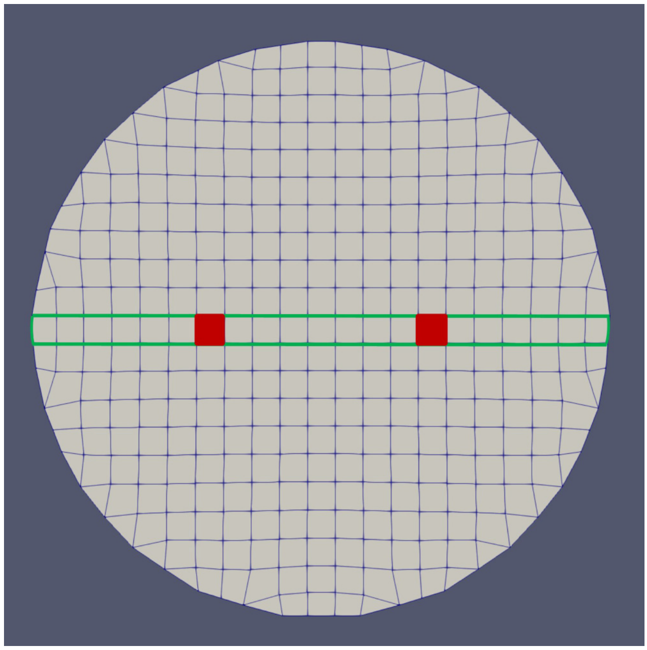

FIG. 2. Horizontal cross section of the CFD mesh used, marking in green the cells used for the central vertical slice through the bed and in red the cells at the bottom of the fluidized bed through which gas was injected to inject bubbles into the bed.

C. Bubble injection

The simulated bubble injection setup was created to match that used experimentally as closely as possible. Through all cells in the base of the fluidized bed, except for two used for bubble injection, gas was flowed at a constant gas velocity equal to the minimum fluidization velocity to barely suspend the particles. This matches the experimental condition of gas injected uniformly at minimum fluidization conditions through a perforated plate except at the two orifices used for bubble injection. Bubbles were injected via two CFD cells highlighted in Fig. 2, with gas velocity nonzero for 30 ms, to match that used in the experiments. Gas velocities were the same in the two orifices in one simulation, to simulate a condition in which the two bubbles were equal in size, and slightly different in another simulation, to simulate one bubble being slightly smaller than the other. In the prior experiments, the bubble injection ports were separated by 80 mm and were circular with a diameter of 7.95 mm. In the simulations, the injection ports were 72.4 mm apart and were square in shape with side length 9.05 mm.

D. MRI measurements

No MRI measurements were performed in this study, but we describe the details of the prior experimental study [4] briefly here and refer readers to other papers for fuller descriptions [4,17]. Rapid imaging of granular flows was achieved using a combination of techniques, as described previously [17]. A specially built 16-channel radiofrequency coil [17] was placed around the fluidized bed and the entire system was placed in a Philip Achieve 3T MRI scanner. Echo planar imaging [18] with the SENSE algorithm [19] was used for rapid imaging of the particle concentration field. This was combined with phase contrast velocimetry [20] to achieve rapid imaging of both the particle concentration and the particle velocity field. Images were taken of a central vertical slice through the bed with a slice thickness of 10 mm.

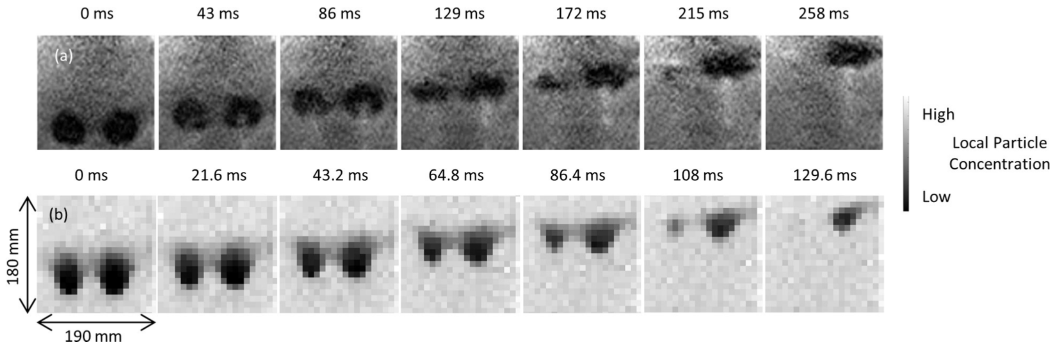

FIG. 3. Time series of images of the void fraction through a central slice of the fluidized bed with side-by-side bubbles injected for 30 ms from (a) MRI experiments from a prior study with gas injection velocity ∼160 m/s through both ports (volumetric flow rate of 0.008 m^3/s through each port), spatial resolution of 3 mm (horizontal) × 3 mm (vertical) with a 10 mm slice and (b) CFD-DEM simulations conducted here with CFD grid size of 9.375 mm, the gas injection velocity of 60 m/s through the left port (volumetric flow rate of 0.0049 m^3/s) and 65 m/s through the right port (volumetric flow rate of 0.0053 m^3/s).

E. Image processing

Images of simulation data of void fraction and gas velocity were produced using Matlab and Paraview. Images of void fraction and gas velocity for a 2D central vertical slice (highlighted in Fig. 2) were produced by importing simulation data into Matlab. 3D images were produced in Paraview by applying a filter to show only CFD cells in which the void fraction was above 0.8 to show the bubbles and using the "streamline" feature to convert the gas velocity field output by the simulation into streamlines.

III. RESULTS AND DISCUSSION

Figure 3 shows [Fig. 3(a)] MRI measurements [4] and [Fig. 3(b)] CFD-DEM simulation predictions of the void fraction over time through a central vertical slice in a case in which both bubbles are injected for 30 ms and the left bubble collapses. In the MRI measurements [Fig. 3(a)], both bubbles had identical injection conditions, and thus the expectation is that the same amount of gas is injected through both ports and bubbles are equal in size. However, image processing of the MRI data in the previous study shows that the left bubble was actually a bit smaller than the right bubble [4]. Thus, in the CFD-DEM simulations, the gas in the left bubble was injected at 60 m/s, while that in the right bubble was injected at 65 m/s, making the left bubble slightly smaller than the right bubble. The injection velocities were different for CFD-DEM and MRI measurements, due in part to the larger area of the simulated injection ports, and the simulated bubbles rose at different velocities than the experimental bubbles with somewhat different shapes. Nevertheless, the simulations qualitatively reproduce the apparent bubble collapse phenomenon, providing confidence in the validity of the model in addition to the multitude of other studies validating CFD-DEM simulations against experiments [6,13,21–24]. Figure 3 demonstrates that CFD-DEM can reproduce the apparent bubble collapse phenomenon observed experimentally; however, the question still remains if the left bubble actually collapsed or if instead it just moved out of the imaging plane. While the CFD-DEM simulations reproduce the collapse phenomenon, the bubbles rise and collapse in the CFD-DEM simulation is significantly more rapidly than in the MRI experiments. The authors attribute this to quantitative inaccuracies in CFD-DEM simulations, most likely introduced by the use of a drag law to couple gas and solids flow, as has been shown in previous studies [13,14] that changing drag laws strongly affects bubble dynamics. These inaccuracies could be avoided by

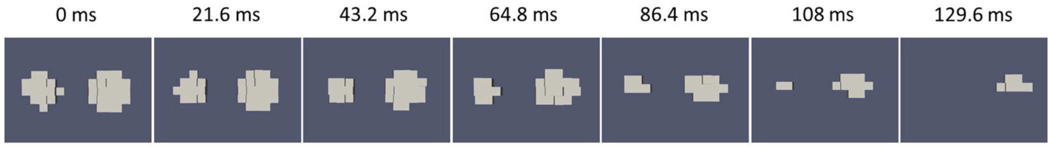

FIG. 4. Time series of 3D renderings of CFD cells from a top view of the fluidized bed showing bubbles rising in the same CFD-DEM simulation shown in Fig. 3(b).

using a smaller CFD grid and directly coupling gas-solid flow via the no-slip boundary condition; however, this would be prohibitively computationally expensive.

Figure 4 shows images from the same simulation as in Fig. 3(b), but this time showing a 3D top view of the bubbles as they rise over time. Figure 4 demonstrates that the left bubble does in fact collapse, and neither bubble moves out of the central plane.

To address the question of the mechanism causing bubble collapse, Fig. 5 shows simulation predictions for the same simulation as in Fig. 3(b), but showing [Fig. 5(a)] the void fraction and [Fig. 5(b)] the gas speed field in a central vertical slice with gas velocity indicated by arrows. Figure 5(c) provides a 3D perspective of the gas flow surrounding the bubbles, with streamlines indicating the gas flow as the bubbles rise over time. These results demonstrate that gas flow below the bubbles is channeled into both bubbles, with more gas flow channeled into the right bubble than the left bubble. This channeling of gas flow is expected due to the higher permeability of bubbles to gas flow than the particulate phase, and greater channeling through the larger bubble can be explained by larger bubbles providing an even easier path for gas to permeate through the fluidized bed. Channeling of gas through bubbles is expected based on Davidson's theory [1] for gas flow around a single bubble, and this theory also demonstrated that this gas flow through the roof of the bubble, not arching, is what allows the bubble roof to maintain its shape as it rises.

To address the question of whether or not a smaller bubble is needed for a bubble to collapse, Fig. 6 shows simulation prediction for bubble injection where both bubbles are injected at 65 m/s. In this case both bubbles form at the same size and rise through the bed without collapsing, indicating

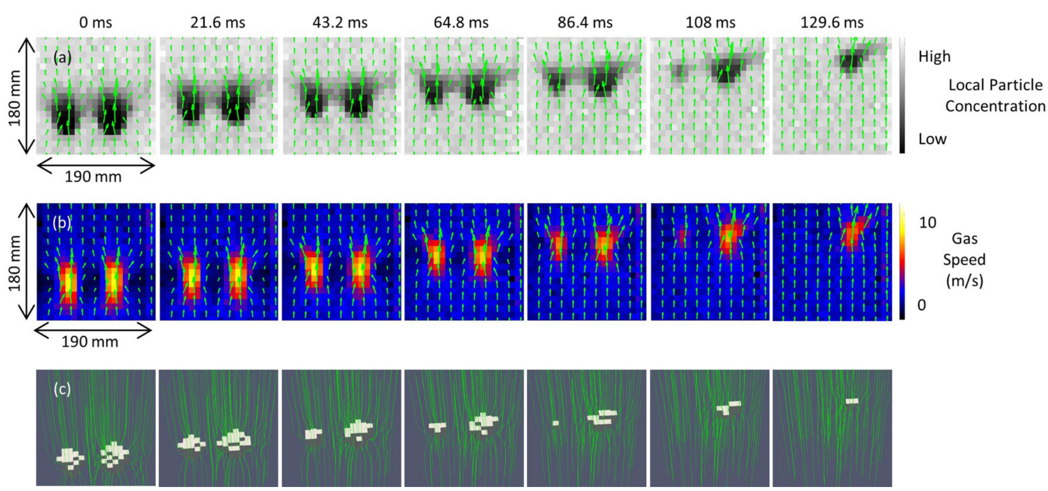

FIG. 5. Images of gas velocity surrounding bubbles for the same CFD-DEM simulation as shown in Fig. 3(b) with CFD grid size of 9.375 mm. (a) The void fraction and (b) the gas speed; both (a) and (b) show a central vertical slice and use arrows to indicate gas velocity. (c) 3D perspective outlining the bubbles and showing streamlines of gas flowing through the bubbles.

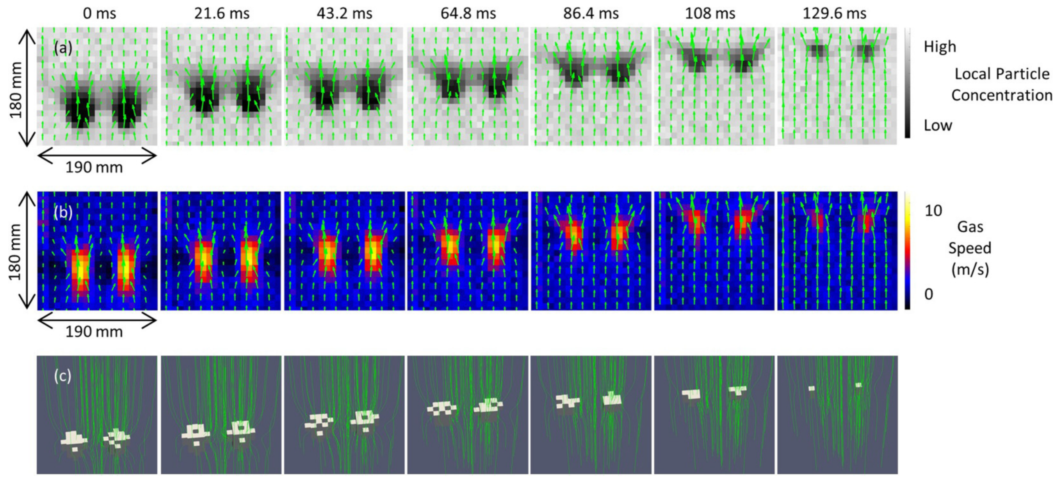

FIG. 6. Time series of images of (a) void fraction, (b) gas speed, and (c) a 3D perspective of bubbles with green arrows and lines indicating gas flow in a central vertical plane from a CFD-DEM simulation with CFD grid size of 9.375 mm and bubbles injected side-by-side for 30 ms with a 65 m/s gas injection velocity through both ports.

that a mismatch in bubble size is critical to collapse. Also, the simulation results show that the collapse phenomenon occurs only when the extent of size difference is beyond a critical value. When the gas injection velocities in the left bubble and right bubbles are 63 m/s and 65 m/s, respectively, both bubbles rise through the bed and no collapse occurs. Figure 7 quantifies the results shown in Figs. 5 and 6. Figure 7(a) demonstrates the total volume of both bubbles for the two injections with ($U_{\mathrm{inj,L}} = 65\,\mathrm{m/s}$, $U_{\mathrm{inj,R}} = 65\,\mathrm{m/s}$) and ($U_{\mathrm{inj,L}} = 63\,\mathrm{m/s}$, $U_{\mathrm{inj,R}} = 65\,\mathrm{m/s}$) are fairly similar throughout the bubble rise process. However, the injection with ($U_{\mathrm{inj,L}} = 60\,\mathrm{m/s}$, $U_{\mathrm{inj,R}} = 65\,\mathrm{m/s}$) has a lower value for the total volume of bubble initially because of the lower amount of injected gas, but then it starts to have a greater value than the other two cases due to the collapse of the left bubble and gas transfer from interstitial flow to the right bubble so that the right bubble maintains its shape and volume and reaches the bed surface. In Fig. 7(b) the volumes of both individual bubbles ($U_{\mathrm{inj,L}} = 65\,\mathrm{m/s}$, $U_{\mathrm{inj,R}} = 65\,\mathrm{m/s}$) are similar to one another as they both grow after the injection, reach a maximum volume, and then start to decrease in size due to gas leakage into the interstitial flow before eventually reaching the bed surface. In the other case, the volume of the bubble with $U_{\mathrm{inj,L}} = 63\,\mathrm{m/s}$ is lower than the volume of the bubble with $U_{\mathrm{inj,R}} = 65\,\mathrm{m/s}$ throughout the rise process, but they both reach the surface of the bed without collapsing. However, when the size difference is increased even more, with injecting the gas into the bubble with $U_{\mathrm{inj,L}} = 60\,\mathrm{m/s}$, and keeping the $U_{\mathrm{inj,R}} = 65\,\mathrm{m/s}$ the same, it can be observed that the left bubble decreases in size faster until its volume reaches zero. However, the right bubble retains a larger volume than in any other case as it reaches the surface of the bed.

Thus, the simulation results confirm the hypothesis from the previous experimental work shown in Fig. 1 that preferential gas channeling toward the larger bubble leads to the collapse of the smaller bubble. As the smaller bubble decreases in size, less and less gas channels into it, demonstrating the instability which causes the collapse. Further, the gas velocity fields and streamlines demonstrate that gas is not transferred directly from the collapsing bubble to the surviving bubble, but rather, gas channels into both bubbles from below and reemerges from the roofs of both bubbles to create a fairly uniform upward gas flow above the bubbles.

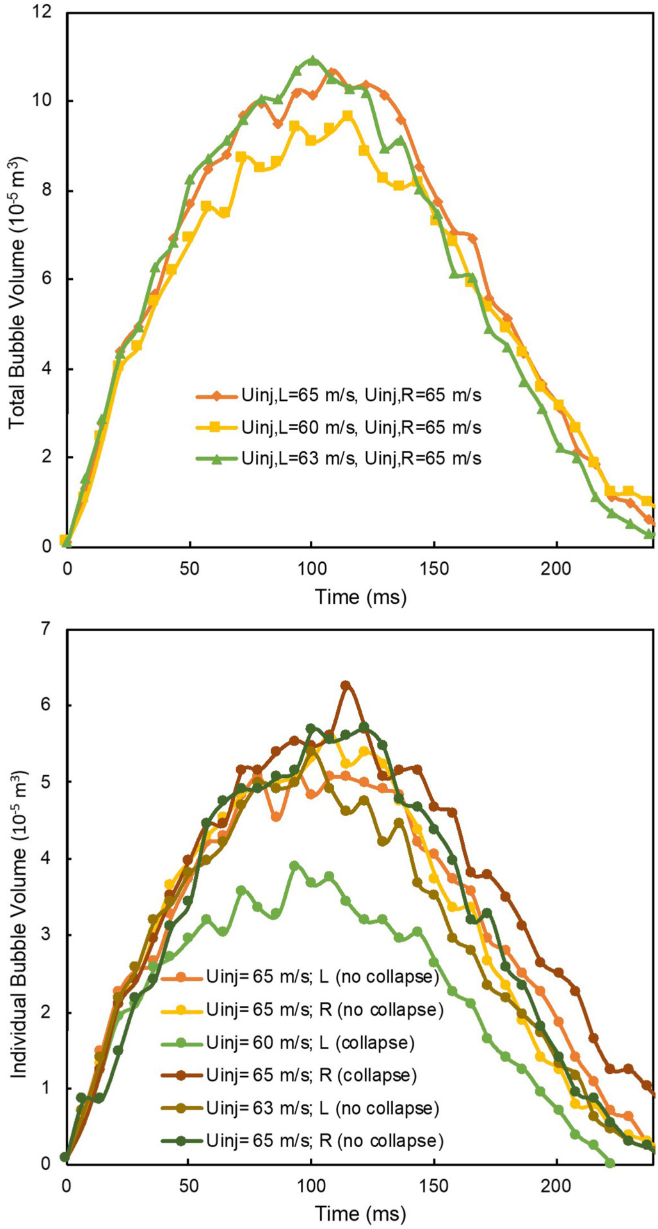

FIG. 7. Bubble volume vs time for two bubbles injected side by side (L = left, R = right) for 30 ms with different gas injection velocity. (a) The total bubble volume from both the right and left bubbles and (b) the individual volume of each bubble.

IV. CONCLUSIONS

CFD-DEM simulations have been shown to reproduce the bubble collapse phenomenon observed in a prior experimental study [4] when two bubbles are injected side-by-side into an incipiently fluidized bed. Simulation results show that the bubble does indeed collapse, rather than move out of the central injection plane, and that the collapsing bubble must be slightly smaller than the surviving bubble for collapse to occur. CFD-DEM simulation predictions of gas velocity confirm the mechanism proposed in the experimental study [4] that gas channels preferentially to a larger bubble, leaving the smaller bubble with insufficient gas flow through it to maintain its shape. Simulation predictions also show that gas flowing out of the collapsing bubble does not flow directly into the surviving bubble.

---

[1] J. F. Davidson and D. Harrison, *Fluidised Particles* (Cambridge University Press, Cambridge, 1963).

[2] R. M. Davies and G. I. Taylor, The mechanics of large bubbles rising through extended liquids and through liquids in tubes, Proc. R. Soc. Lond. Ser. Math. Phys. Sci. **200**, 375 (1950).

[3] J. S. Dennis, Properties of stationary (bubbling) fluidized beds relevant to combustion and gasification systems, in *Fluidized Bed Technologies for Near-Zero Emission Combustion and Gasification*, edited by F. Scala (Woodhead Publishing, Cambridge, 2013), Vol. 77.

[4] C. M. Boyce, A. Penn, A. Padash, M. Lehnert, K. P. Pruessmann, and C. R. Müller, Anomalous collapse of interacting bubbles in a fluidized bed: A magnetic resonance imaging study, Phys. Rev. Fluids **4**, 034303 (2019).

[5] T. W. Asegehegn, M. Schreiber, and H. J. Krautz, Investigation of bubble behavior in fluidized beds with and without immersed horizontal tubes using a digital image analysis technique, Powder Technol. **210**, 248 (2011).

[6] Y. Tsuji, T. Kawaguchi, and T. Tanaka, Discrete particle simulation of two-dimensional fluidized bed, Powder Technol. **77**, 79 (1993).

[7] P. A. Cundall and O. D. L. Strack, A discrete numerical model for granular assemblies, Géotechnique **29**, 47 (1979).

[8] T. B. Anderson and R. Jackson, Fluid mechanical description of fluidized beds. Equations of motion, Ind. Eng. Chem. Fundam. **6**, 527 (1967).

[9] C. Y. Wen and Y. H. Yu, A generalized method for predicting the minimum fluidization velocity, AIChE J. **12**, 610 (1966).

[10] C. Goniva, C. Kloss, N. G. Deen, J. A. M. Kuipers, and S. Pirker, Influence of rolling friction on single spout fluidized bed simulation, Particuology **10**, 582 (2012).

[11] H. G. Weller, G. Tabor, H. Jasak, and C. Fureby, A tensorial approach to computational continuum mechanics using object-oriented techniques, Comput. Phys. **12**, 620 (1998).

[12] C. Kloss, C. Goniva, A. Hager, S. Amberger, and S. Pirker, Models, algorithms and validation for opensource DEM and CFD-DEM, Prog. Comput. Fluid Dyn. Int. J. **12**, 140 (2012).

[13] C. M. Boyce, A. Ozel, N. P. Rice, G. J. Rubinstein, D. J. Holland, and S. Sundaresan, Effective particle diameters for simulating fluidization of non-spherical particles: CFD-DEM Models vs. MRI measurements, AIChE J. **63**, 2555 (2017).

[14] C. R. Müller, D. J. Holland, A. J. Sederman, S. A. Scott, J. S. Dennis, and L. F. Gladden, Granular temperature: Comparison of magnetic resonance measurements with discrete element model simulations, Powder Technol. **184**, 241 (2008).

[15] S. Radl and S. Sundaresan, A drag model for filtered Euler-Lagrange simulations of clustered gas-particle suspensions, Chem. Eng. Sci. **117**, 416 (2014).

[16] C. M. Boyce, D. J. Holland, S. A. Scott, and J. S. Dennis, Limitations on fluid grid sizing for using volume-averaged fluid equations in discrete element models of fluidized beds, Ind. Eng. Chem. Res. **54**, 10684 (2015).

[17] A. Penn, T. Tsuji, D. O. Brunner, C. M. Boyce, K. P. Pruessmann, and C. R. Müller, Real-time probing of granular dynamics with magnetic resonance, Sci. Adv. **3**, e1701879 (2017).

[18] M. K. Stehling, R. Turner, and P. Mansfield, Echo-planar imaging: Magnetic resonance imaging in a fraction of a second, Science **254**, 43 (1991).

[19] K. P. Pruessmann, M. Weiger, M. B. Schneidegger, and P. Boesiger, SENSE: Sensitivity encoding for fast MRI, Magn. Reson. Med. **42**, 952 (1999).

[20] P. T. Callaghan, *Principles of Nuclear Magnetic Resonance Microscopy* (Oxford University Press, Oxford, 1991).

[21] N. G. Deen, M. Van Sint Annaland, M. A. Van der Hoef, and J. A. M. Kuipers, Review of discrete particle modeling of fluidized beds, Chem. Eng. Sci. **62**, 28 (2007).

[22] C. M. Boyce, J. F. Davidson, D. J. Holland, S. A. Scott, and J. S. Dennis, The origin of pressure oscillations in slugging fluidized beds: Comparison of experimental results from magnetic resonance imaging with a discrete element model, Chem. Eng. Sci. **116**, 611 (2014).

[23] C. P. McLaren, T. M. Kovar, A. Penn, C. R. Müller, and C. M. Boyce, Gravitational instabilities in binary granular materials, Proc. Natl. Acad. Sci. USA **116**, 9263 (2019).

[24] C. M. Boyce, D. J. Holland, S. A. Scott, and J. S. Dennis, Adapting data processing to compare model and experiment accurately: A discrete element model and magnetic resonance measurements of a 3D cylindrical fluidized bed, Ind. Eng. Chem. Res. **52**, 18085 (2013).